THE JOURNAL OF PHYSICAL CHEMISTRY A

Feature Article

pubs.acs.org/JPCA

Weakly Bound Clusters in Astrochemistry? Millimeter and Submillimeter Spectroscopy of *trans*-HO_3 and Comparison to Astronomical Observations

Luyao Zou, Brian M. Hays, and Susanna L. Widicus Weaver*

Department of Chemistry, Emory University, Atlanta, Georgia, United States

Supporting Information

ABSTRACT: The emergence of chemical complexity during star and planet formation is largely guided by the chemistry of unstable molecules that are reaction intermediates in terrestrial chemistry. Our knowledge of these intermediates is limited by both the lack of laboratory studies and the difficulty in their astronomical detection. In this work, we focus on the weakly bound cluster HO_3 as an example of the connection between laboratory spectroscopic study and astronomical observations. Here, we present a fast-sweep spectroscopic technique in the millimeter and submillimeter range to facilitate the laboratory search for *trans*-HO_3 and DO_3 transitions in a discharge supersonic jet and report their rotational spectra from 70 to 450 GHz. These new measurements enable full determination of the molecular constants of HO_3 and DO_3. We also present a preliminary search for *trans*-HO_3 in 32 star-forming regions using this new spectroscopic information. HO_3 is not detected, and column density upper limits are reported. This work provides additional benchmark information for computational studies of this intriguing radical, as well as a reliable set of molecular constants for extrapolation of the transition frequencies of HO_3 for future astronomical observations.

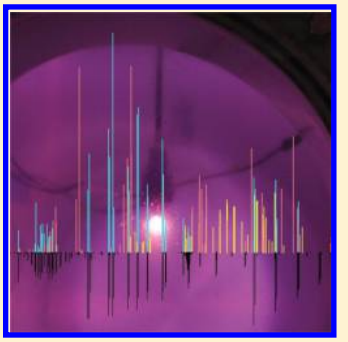

INTRODUCTION

The chemical complexity on Earth is extraordinary when compared to the universe, where H_2 is by far the most abundant molecular species. The low densities and temperatures of space limit the chemistry that can occur in interstellar environments, and observations show that "terrestrial" chemical complexity only begins to emerge as stars and planets form. Few studies have focused on the chemical processes involved in star and planet formation but rather used molecules to trace the physical conditions. We approach this problem from an astro*chemistry* perspective, rather than an astro*physical* one. Our focus is on the reaction intermediates that drive the chemistry, such as radicals, ions, and other transient molecules. The fundamental question to be answered by our research is *How does chemical complexity emerge from the simple chemistry observed in space?*

In this work we examine the possibility of the existence of weakly bound clusters in space through laboratory and observational studies of HO_3. HO_3 is chemically related to molecular oxygen, which presents a puzzle for astrochemists. O_2 has surprisingly only been detected in a few sources,[1−4] despite the relatively large fractional abundance of atomic oxygen relative to hydrogen. Identifying the carrier(s) of oxygen in dense molecular clouds encourages new reaction mechanisms to be proposed. Silicates, CO, and water ice are the major reservoirs of oxygen in these environments, but they do not fully explain the low molecular oxygen abundance that is observed in dense clouds.[5] Other possible oxygen reservoirs must be investigated. Here we explore whether weakly bound clusters could play important roles in oxygen chemistry in interstellar clouds.

Strongly bound clusters, such as protonated molecular ions like H_3^+, HCO^+, and N_2H^+, play central roles in both terrestrial and interstellar chemistry, and their existence has been unambiguously supported by astronomical observations.[6] Weakly bound clusters, however, are important reaction intermediates in terrestrial chemistry, but they have been discounted as important intermediates in interstellar chemistry because the low densities in interstellar clouds do not favor their formation. Nonetheless, the question of their possible existence in interstellar clouds is intriguing. Indeed, if a three-body collision is required to form such a cluster, as is typical under terrestrial conditions, such a reaction is unlikely in interstellar environments. However, Klemperer and Vaida[6] suggest that weakly bound clusters whose binding energy is ∼5 kcal·mol^{-1} are still possible interstellar species because they can form via radiative association reactions, which are common in interstellar environments. In addition to radiative association in the gas phase, weakly bound clusters could also possibly form on interstellar or protoplanetary ices. Specifically for HO_3, experiments have shown that it can be produced in cold water ice rich in O_2 under proton[7] or electron[8] bombardment. The latest experimental upper limit of HO_3 binding energy is 3 kcal·mol^{-1},[9] whereas the theoretical estimation lies between 1.8[10] and 2.8[11] kcal·mol^{-1}. HO_3 may therefore be produced within

Received: October 1, 2015
Revised: November 23, 2015
Published: December 28, 2015

DOI: 10.1021/acs.jpca.5b09624
J. Phys. Chem. A 2016, 120, 657−667

and survive the sublimation of interstellar ices below 100 K. If detected, clusters such as HO_3 could dramatically change the current understanding of the roles of three-body collisions, radiative association reactions, and sublimation in astrochemistry.

The identification of HO_3 via its rotational transitions cannot be achieved without supporting laboratory measurements. We focus here on the millimeter and submillimeter spectrum of HO_3. Although rotational spectra of *trans*-HO_3 are available in the microwave range,[12,13] extrapolation to the millimeter−submillimeter wavelength range may be subject to large uncertainties. Therefore, our experimental measurements of HO_3 transitions at these wavelengths will aid in the search for this cluster in space. Once the HO_3 rotational spectrum is measured, we can apply similar techniques to examine other clusters of astrochemical interest.

In addition to its possible importance in astrochemistry, HO_3 is also of great interest in atmospheric chemistry and theoretical chemistry. It is a challenging target in both experimental and computational studies. In experimental studies, its potential role in shaping the HO_x cycle that controls the atmospheric O_2 budget was proposed (see Murray et al.[14] and references therein) but then discarded based on more accurate experimental results.[9] In computational studies, HO_3 is a sensitive benchmark for theoretical methods as its experimentally measured properties can rarely be simultaneously reproduced by a single theoretical method.

The experimental measurement of the dissociation energy of HO_3 determines its importance in atmospheric chemistry. The value 10(5) kcal·mol^{-1} determined from proton and electron transfer experiments[15,16] was unreliable due to large experimental uncertainty and large discrepancy from theoretical calculations. From infrared−UV action spectroscopy, Derro et al. estimated the upper limit of the dissociation energy of HO_3 to be 5.32 kcal·mol^{-1}, by measuring the maximum energy of dissociated OH.[17] Le Picard et al.[9] further refined the upper limit of the HO_3 dissociation energy to be 2.97(7) kcal·mol^{-1}, which was derived from a kinetics model based on laser-induced fluorescence (LIF) decay measurements of OH at various temperatures and O_2 concentrations. Therefore, the originally postulated contribution of HO_3 to atmospheric OH depletion was discarded.

Spectroscopic studies of HO_3 have been primarily conducted in the infrared. Early spectroscopic investigations of HO_3 after its first detection in mass spectrometry[18] include infrared experiments in an Ar matrix[19] and water ice.[7,8] Rotationally resolved infrared spectra were first obtained by infrared−UV action spectroscopy in a supersonic jet,[17,20−22] where an infrared laser was used to pump the radical, while the dissociation product OH was probed via LIF from its UV excitation. Several rotationally resolved bands were unambiguously assigned to *trans*-HO_3.[17] Vibrational bands of *trans*-DO_3 were also measured.[17,22]

Additional rotational spectroscopic studies using Fourier Transform Microwave (FTMW) spectroscopy have shown that HO_3 possesses an extremely long center O−O bond.[12,13] In these experiments, HO_3 was formed in a pulsed discharge supersonic expansion comprised of a mixture of O_2 and water vapor or H_2 diluted in Ar. Spectra of HO_3 and DO_3 were measured by Suma et al., and spectra of its three ^{18}O isotopologues were measured by McCarthy et al., who also reported a more efficient discharge production mechanism of HO_3 using H_2 instead of H_2O as a precursor. Transitions for HO_3 were measured up to 80 GHz. Empirical structural information for *trans*-HO_3 was derived from the experimental rotational constants of the five isotopologues retrieved from the microwave spectra, by assuming a planar geometry.[13] The empirical center O−O bond was very long (1.684 Å), while the O−H bond was much shorter (0.913 Å) than that in free OH (0.970 Å). As the authors pointed out, however, the empirical bond length r_0 is not directly comparable to the theoretical equilibrium value r_e, due to the effect of the vibrational wavefunction in the ground state. A recent dipole moment measurement for *trans*-HO_3 in a He nanodroplet further illustrated the large discrepancy between theoretical calculated properties with experimental measurements, as well as the sensitive dependence of the radical's property on its geometry estimation.[23]

It is worthwhile to mention that the existence of *cis*-HO_3 is perplexing. A broad infrared band containing no rotational structure was tentatively assigned to the *cis*- conformer,[17,20−22] but the validity of this assignment is questionable because both microwave studies claimed no detection of *cis*-HO_3 after careful searches.[12,13] As Raston et al. suggested based on their He nanodroplet study, it is possible that there is only one vibrationally averaged structure of HO_3, and the broad infrared band arises from HO_3−$(O_2)_n$ complexes.[24]

Along with these experimental efforts, theoretical calculations have been extensively conducted to reproduce the experimentally measured molecular geometry and dissociation energy, to construct the potential energy surface, and to analyze the dissociation channels.[10,11,25−36] Despite this fact, none of these studies can thus far simultaneously reproduce every experimentally measured aspect of this radical. This is not only due to the complexity of the HO_3 system itself, but also to the difficulty of direct comparison of theoretical results with experimental values. The comparison of geometry, dipole moment, and dissociation energy for the ground vibrational state of HO_3 relies greatly on the estimation of the anharmonic multidimensional potential energy surface as well as the vibrational−rotational interaction. For example, the torsional potential between the *trans* and *cis* conformer (if it does exist) of HO_3 largely determines the form of the rovibronic wave functions. The torsional barrier is estimated to be ∼340 cm^{-1},[33] based on the infrared−UV action spectroscopy results.[17] A more recent six-dimensional potential energy surface[10] showed strong coupling between multiple vibrational modes, which all have impact on the estimation of the difference between the theoretical equilibrium geometry and the empirical geometry. Much theoretical and experimental work remains to fully understand the HO_3 system.

Here, we report the measurement of pure rotational spectra of HO_3 and DO_3 from 70 to 450 GHz. These new measurements access more K_a levels than the microwave studies, thus providing sufficient information to empirically fit all quartic centrifugal distortion constants using a standard asymmetric top Hamiltonian. In addition to the observed HO_3 and DO_3 transitions, we found numerous unidentified lines. In conjunction with these experiments, we benchmarked a new fast-sweep spectral scanning technique that facilitated the laboratory characterization of HO_3. We then compared these experimental results with observational spectra to search for HO_3 in 32 star-forming regions and estimated upper limits of HO_3 abundance in these astronomical sources.

DOI: 10.1021/acs.jpca.5b09624
J. Phys. Chem. A 2016, 120, 657−667

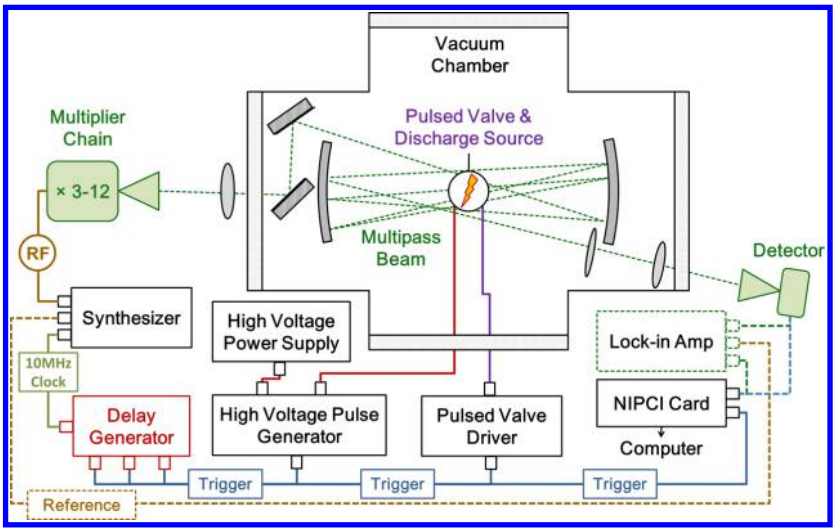

Figure 1. Schematic of the experimental setup.

EXPERIMENTAL DETAILS

Production of HO_3 and DO_3. The HO_3 radical was produced in a pulsed high-voltage discharge in a supersonic expansion of a gas mixture of O_2, H_2, and Ar (NexAir, ultrahigh purity). The seeding gases O_2 and H_2 were premixed at a flow ratio of 3:2 and then diluted to 10% in Ar before being sent into a pulsed valve (Parker Hannifin, Series 9 general valve). The valve operated at a repetition rate between 20 and 25 Hz with ∼1 ms opening time, which led to a total gas flow rate of 700−850 sccm and an equilibrium chamber pressure of ∼5 Pa. Gas flow was controlled by a set of mass flow controllers (MKS 1179A, 100 sccm maximum for seeding gases and 5000 sccm maximum for the buffer gas) and a four-channel flow rate readout (MKS Type 247). The gas mixture was held at a pressure of 600 kPa above atmosphere behind the pulsed valve. The gas mixture passed through a custom-built discharge source adapted from the design of McCarthy and co-workers[37,38] before expanding into the vacuum. The discharge source used two copper electrodes, separated from each other by 4.8 mm using Teflon washers. Voltage was applied to the electrode closer to the pulsed valve, while the other electrode was grounded. Additional Teflon spacers separated the grounded electrode and source orifice by 15.9 mm to provide sufficient three-body collision stabilization. The discharge voltage was set at +900 V using a high-voltage power supply (Spellman, SL2PN2000) and pulsed by a pulse generator (Directed Energy Inc., PVX-4150). A 10 kΩ ballast resistor constrained the discharge current below 5 mA. The voltage rose simultaneously with the pulsed valve trigger signal, and it lasted for 2.2−2.5 ms. All pulses were triggered using a standard 5 V TTL output from a four-channel delay generator (Stanford Research Systems, DG645). DO_3 was produced under identical conditions, but using D_2 (Cambridge Isotopes Laboratories, 99.8% D_2, 0.2% HD) in place of H_2.

A schematic of the experimental setup is shown in Figure 1. The expanding jet was probed by a seven-pass millimeter−submillimeter spectrometer that was oriented perpendicular to the expansion trajectory. The optical arrangement was based on the designs of Kaur et al.[39] and Laas et al.[40] Two spherical mirrors (Edmund Optics, 15.24 cm diameter and 15.24 cm focal length, NT32−836) spaced by roughly 60 cm were used. The multipass beam was focused into a ∼2.5 cm area in the center of the mirrors, located 2.5 cm underneath the discharge source. The fine-tuning of the discharge source location relative to the beam was optimized for HO_3 detection by maximizing the intensity of the strongest transition of HO_2, the molecular precursor of HO_3.[13] The millimeter−submillimeter beam was generated by multiplication of the 25−45 GHz output from a signal generator (Agilent Technology, E8257D PSG with the options 1EA, UNU, 550, and UNT). Multiplication was achieved using a frequency multiplier chain (Virginia Diodes Inc., S197(b) with WR8 tripler for 105−135 GHz and S197(c) with WR10 tripler plus WR5.1 doubler, WR3.4 tripler, and WR2.2 doubler for other frequency bands) to generate output frequencies in the range of 75−450 GHz.

Detection of Molecular Signal. Two detection schemes were applied in this experiment: a conventional lock-in amplifier scan and a new fast-sweep technique. In both detection methods, the output signal from the spectrometer was detected by either a zero-biased detector (Virginia Diodes Inc., WR10 and WR8.0) for frequencies below 135 GHz, or an InSb hot electron bolometer (QMC, Ltd., QFI/XBI) for frequencies above 135 GHz.

For conventional lock-in detection, the output signal from the detector was processed by a lock-in amplifier (Stanford Research Systems SR830) using 2f detection at a time constant of 0.1 ms. The radiation from the synthesizer was frequency modulated by a 30 kHz oscillating sine wave that deviated off the carrier frequency by ±75 kHz. A scanning step size of 50 kHz was used. The output from the lock-in amplifier was then recorded by a fast digitizer card (National Instruments, PCI-5124) and was numerically integrated to recover the line shape. For fast-sweep acquisition, described in more detail below, the output from the bolometer was directly recorded by the same digitizer card.

The goal of the new fast-sweep technique implemented in this experiment is to speed up the search for unknown transitions of HO_3 without introducing additional instrumentation. The traditional point-by-point lock-in scan significantly constrains the data acquisition speed in a pulsed experiment with low duty cycle. For example, a spectrum of 10 MHz bandwidth with 100 averages under our experimental conditions will take ∼1000 s. Other broadband data acquisition techniques are available in the millimeter−submillimeter wavelength range,[41−43] but unfortunately they require signifi-

DOI: 10.1021/acs.jpca.5b09624
J. Phys. Chem. A 2016, 120, 657−667

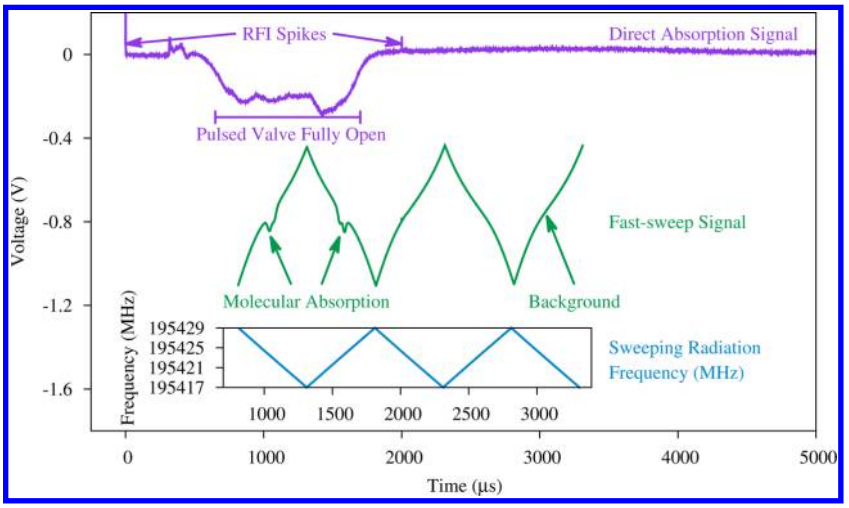

Figure 2. Single frequency time scan over HO_2 $3_{0,3} \leftarrow 2_{0,2}$ transitions (purple trace) and fast-sweep signal in five half-cycles centered on the HO_2 transitions at 195 423 MHz (green trace). The inset plot (blue trace) represents the frequency sweeps in real time.

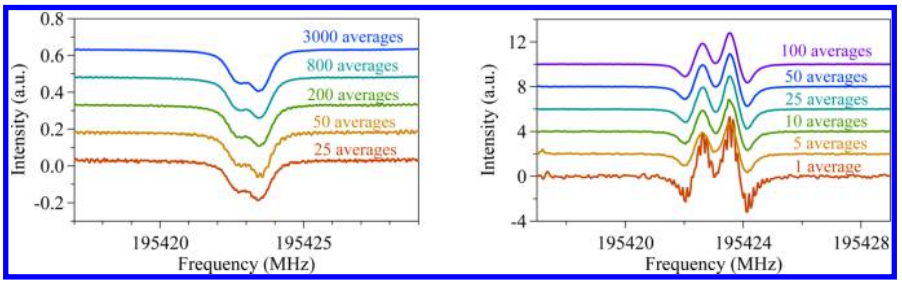

Figure 3. Comparison of spectra recovered from fast-sweep technique (left) and conventional lock-in detection (right).

cant instrumentation investment. We therefore developed a new approach that enabled faster data acquisition without requiring the purchase of new equipment. The fast-sweep technique introduced in this experiment increased the speed of spectral acquisition by 2 orders of magnitude using the identical instruments described in the previous subsection.

The fast-sweep acquisition was achieved by utilizing the internal triangle-wave frequency modulation from the Agilent synthesizer described above. The SRS delay generator was phased-locked to the synthesizer's internal 10 MHz clock to ensure phase stability. The triangle-wave modulation was set to generate a ±1 MHz frequency deviation off the carrier center frequency at 1 kHz rate. The multiplier chain (with multiplying factor 6−12 in this experiment) further multiplied the frequency bandwidth to ±6−12 MHz, which yielded a 12−24 MHz wide linear frequency sweep. This frequency sweep was timed to coincide with the molecular pulse from the pulsed valve, yielding coverage of an entire spectral line in the sweeping bandwidth, as well as a background spectrum immediately after the pulsed valve was closed. An example of the spectra produced by this fast sweeping method is shown in Figure 2. The top spectrum shows a time trace recorded for a frequency centered on one of the hyperfine components of the $3_{0,3} \leftarrow 2_{0,2}$ transition of HO_2 at 195 423 MHz. The spectrum traces the molecular pulse coming from the pulsed valve, providing time information for the production of the target molecule. Two radio frequency interference (RFI) spikes mark the beginning and end of the electrical discharge. The full open time of the valve was usually 0.7 ms, though this varied slightly depending on valve conditions. The middle spectrum shows the fast sweep spectrum as the frequency swept linearly through the same HO_2 transition. The curvature of the sweep was caused by the combination of the power variation from the multiplier chain, the standing waves in the spectrometer, and the sensitivity profile of the detector, which were all frequency-dependent. The inset plot shows the electronic modulation output from the synthesizer, with voltage scaled to the radiation frequency output. The downward slope of this trace in the first half-cycle indicates that the sweep initiated with decreasing frequency in this example. The detector was not sensitive to the direction of this sweep, so this modulation output was recorded in advance as a reference for frequency calibration.

Five sweep half-cycles were recorded in each data acquisition. The delay time of the first sweep half-cycle was tuned via the delay generator so that it coincided with the peak number density of the target molecule in the valve pulse. To avoid signal contamination from molecular residual (usually in the second half-cycle) and RFI (usually in the third or fourth half-cycle), the fifth half-cycle was used as a clean background and was subtracted from the first half-cycle during data analysis.

Postprocessing of the sweep data was performed by a custom-built Python3.4 script with the assistance of Numpy1.8 and Scipy0.15 modules (www.python.org, www.numpy.org, and www.scipy.org). The script first mapped time to radiation frequencies by combining the prerecorded modulation output (i.e., the inset plot in Figure 2) and bandwidth information. The next step was to reshape the data array, taking the fifth sweep as the background signal and subtracting it from the first one. Lastly, the background-subtracted molecular signals at all center frequencies within the same data file (1 GHz range in this experiment) were stitched together to create a spectrum,

DOI: 10.1021/acs.jpca.5b09624
J. Phys. Chem. A 2016, 120, 657−667

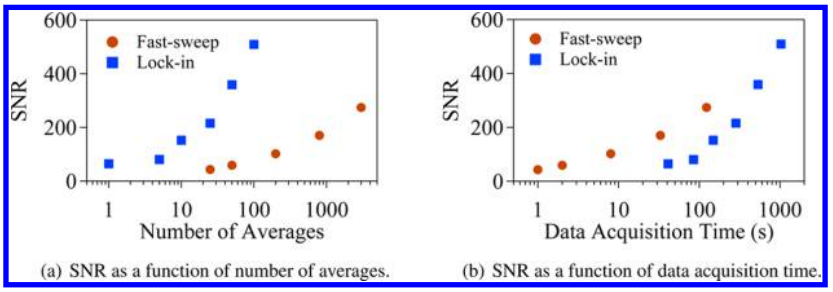

Figure 4. Comparison of SNR between fast-sweep spectra and point-by-point lock-in spectra.

which was subject to additional linear and spline baseline removal processes.

RESULTS

Benchmark of Fast-Sweep. The fast-sweep spectra recovered after frequency calibration and background subtraction of Figure 2 are shown in the left panel of Figure 3, together with the spectra in the same frequency range from conventional lock-in detection in the right panel for comparison. The fast-sweep signal has a Voigt line shape, while the lock-in line shape is the second derivative of the fast-sweep line shape. Various numbers of averages were taken to trace the improvement in signal-to-noise ratio (SNR). Both detection methods present a square-root improvement of SNR as the number of averages increases. Figure 4 further compares the improvement of SNR in both detection methods as a function of number of averages and data acquisition time. At the same number of averages, the lock-in detection gives higher SNR than the fast-sweep, which is not surprising. The time it takes, however, is also much longer than the fast-sweep. For example, using the lock-in takes over 10 times longer than the fast sweep for an SNR of 100. As a result, the fast-sweep is well-suited for fast broadband searches for strong unknown transitions. However, the lock-in detection is more appropriate for detecting weaker transitions in a reasonable amount of averages and given sufficiently accurate knowledge of the transition frequency.

HO_3 and DO_3 Detection. The detection of HO_3 below 170 GHz was straightforward based on the extrapolation of transition frequencies from previous microwave studies,[12,13] once the discharge and gas mixture conditions were optimized for HO_3 production. The transition frequencies observed directly coincided with the extrapolation. Difficulty was experienced for the spectral search above 170 GHz. With the assistance of the fast-sweep technique, large frequency shifts from the extrapolation were observed. For transitions from 170 to 320 GHz, the shift was ~35 MHz, while for transitions above 320 GHz, the shift was ~170 MHz. Sample spectra from the fast-sweep experiment are shown in Figure 5. The frequency shifts compared with extrapolations from microwave data are readily seen.

Each new transition observed in the fast-sweep acquisitions was confirmed using lock-in detection and then fitted by a second derivative Gaussian function to retrieve its transition frequency. Additionally, weaker HO_3 transitions that were ambiguous in the fast-sweep data were sought using the lock-in detection. A total of 38 new lines for HO_3 with 118 resolved hyperfine components were measured in the range from 70 to 450 GHz. The highest J level observed was $J = 7$. The complete list of assignments can be found in the Supporting Information. A computer-generated stick spectrum based on the second-derivative Gaussian fit showing all newly measured transitions of HO_3 is plotted in the top panel of Figure 6. The intensities are proportional to the integrated intensities of measured transitions. DO_3 transitions were also measured using the same procedure. A total of 44 new lines were recorded. Unfortunately, because of the heavier nuclear mass of deuterium, the hyperfine splitting of most lines was not resolved, except for the partially resolved $2_{2,1} \leftarrow 2_{1,2}$ transition. The full stick spectrum is plotted in the lower panel of Figure 6. A scaling factor based on the lock-in amplifier sensitivity was considered for DO_3 but not HO_3. Since the experimental condition details varied day by day, the power fluctuation due to the standing waves in the spectrometer was difficult to calibrate. Therefore, no further power normalization was applied.

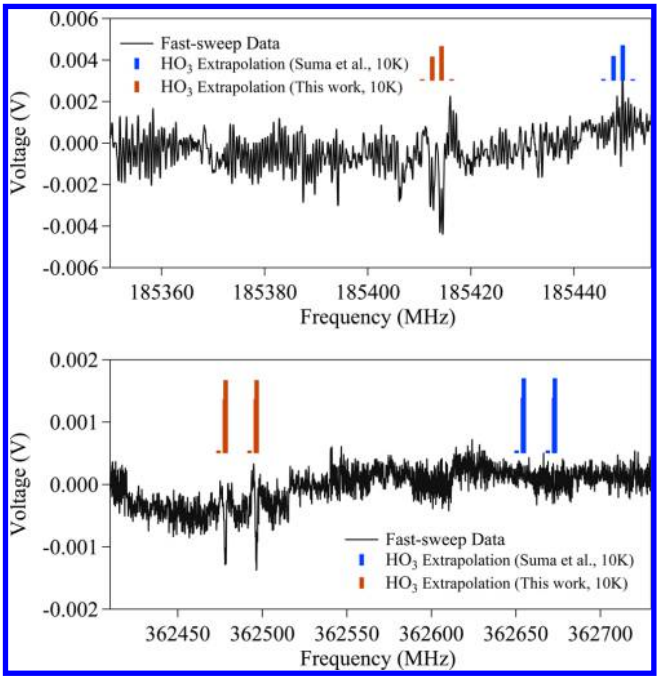

Figure 5. Fast-sweep detection of HO_3 at 185 and 362 GHz. Spectral simulations were generated at 10 K rotational temperature using reported molecular constants from either the previous study (blue) or the current study (orange).

The molecular constants were fitted using the SPFIT program in the CALPGM suite[44] using Watson's A reduced Hamiltonian, including centrifugal distortion, spin-rotation interaction and associated centrifugal distortion, magnetic dipole−dipole hyperfine splitting, and electric quadrupole hyperfine splitting for deuterium. For unresolved HO_3 hyperfine structure, the same center frequency was assigned to the two strongest hyperfine components. For DO_3, the

DOI: 10.1021/acs.jpca.5b09624
J. Phys. Chem. A 2016, 120, 657−667

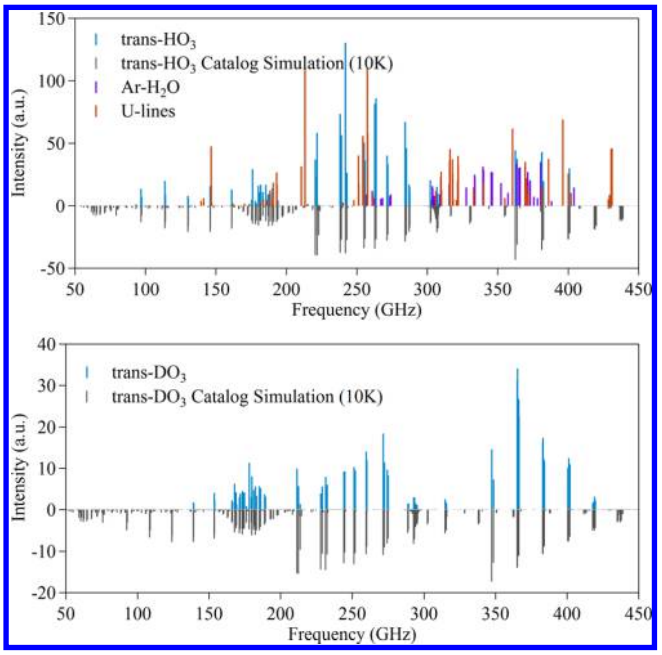

Figure 6. Stick spectra of all new measured HO_3 and DO_3 transitions. Transitions identified to be Ar−H_2O and unidentified lines are also included. Intensities are proportional to the integrated intensities of measured transitions and are calibrated for the sensitivity level of the lock-in amplifier for DO_3 but not HO_3. No power normalization was applied.

strongest three hyperfine components were assigned to the same frequency. The transitions reported by Suma et al.[12] in the microwave range were also included in the fit. Only the molecular constants with statistical significance were included in the fit. The hyperfine tensor element T_{cc} was fixed at $-T_{aa}-T_{bb}$, while χ_{cc} was fixed at $-\chi_{aa}-\chi_{bb}$ to ensure the traceless property of the T and χ matrices. We assumed a uniform 5 kHz frequency uncertainty for the microwave data from Suma et al. and a uniform 50 kHz frequency uncertainty for the data from this study based on the spectral resolution. The root-mean-square (rms) of the fit is 0.050 MHz for HO_3 and 0.051 MHz for DO_3, both of which agree well with the frequency uncertainty in this work. The results of this analysis are compared to previous studies in Tables 1 and 2. The final fit files for HO_3 and DO_3 are also included as Supporting Information.

Using the new spectroscopic constants determined in Tables 1 and 2, we updated the HO_3 and DO_3 spectral predictions using the SPCAT program in the CALPGM suite.[44] For these predictions, the a and b components of the electric dipole moment were set at the experimental values of μ_a = 0.61 D, μ_b = 1.48 D for *trans*-HO_3, and μ_a = 0.62 D, μ_b = 1.52 D for *trans*-DO_3.[23] These new spectral catalogs were used to simulate spectra assuming a rotational temperature of 10 K for comparison to the experimentally measured spectra, shown in Figures 5 and 6. The HO_3 catalog was also used to compare with astronomical observations, which will be discussed in more detail below.

New Spectral Features. Along with the detection of HO_3, we also found a set of new discharge-dependent spectral features using the fast-sweep technique. Follow-up lock-in detections were also conducted to confirm the discovery of new spectral lines. These lines are also plotted in Figure 6 along with the HO_3 lines. One of the molecular carriers was identified to be the Ar−H_2O dimer; these lines, marked in purple in Figure 6, disappeared with substitution of He buffer gas in place of Ar. However, Ar−H_2O does not fully explain all of the unidentified lines measured in this experiment. Additional analysis is required before the carrier(s) of these lines is identified.

DISCUSSION

The search for HO_3 transitions above 170 GHz was complicated due to the large frequency shifts relative to the

Table 1. Comparison of Spectroscopic Parameters of *trans*-HO_3 from This Study and Results[a] from Suma et al.[12]

constants (MHz)	this study	Suma etal.[12]	difference
A_0	70781.118 69(136)	70778.1652(24)	2.9535(28)
B_0	9987.3873(61)	9986.9501(11)	0.4372(62)
C_0	8749.7284(59)	8750.1580(11)	−0.4296(60)
$\Delta_N \times 10^3$	47.5200(223)	46.461(30)	1.059(37)
Δ_{NK}	0.149167(123)	0.15335(40)	−0.00418(42)
Δ_K	2.956094(237)		
$\delta_N \times 10^3$	6.1406(116)	6.11(41)	0.031(43)
δ_K	0.21649(298)		
ϵ_{aa}	−1252.6932(42)	−1252.5858(58)	−0.1074(72)
ϵ_{bb}	−106.25192(198)	−106.2551(26)	−0.0032(33)
ϵ_{cc}	−3.49564(187)	−3.4954(24)	−0.0002(30)
$\lvert\epsilon_{ab} + \epsilon_{ba}\rvert/2$	42.503(80)	42.45(11)	0.05(14)
a_F	3.66102(240)	3.6587(30)	0.0023(38)
T_{aa}	8.4792(46)	8.4828(59)	−0.0036(75)
T_{bb}	−6.8512(45)	−6.8533(56)	0.0021(72)
$\Delta_N^S \times 10^3$	0.987(75)	1.00(10)	−0.01(12)
Δ_{NK}^S	0.05626(85)	0.0544(15)	0.018(17)
Δ_K^S	0.10421(179)		
Δ^b	0.0176	0.0123	0.0053
fitted transitions	180	62	
rms (MHz)	0.050	0.0054	

[a]1σ uncertainties in the unit of the last significant digit are included in parentheses. [b]Inertial defect (amu·Å^2).

DOI: 10.1021/acs.jpca.5b09624
J. Phys. Chem. A 2016, 120, 657−667

Table 2. Comparison of Spectroscopic Parameters of *trans*-DO_3 from This Study and Results[a] from Suma et al.[12]

constants (MHz)	this study	Suma et al.[12]	difference
A_0	67859.764 12(114)	67857.3708(30)	2.3933(32)
B_0	9448.9011(46)	9448.5330(13)	0.3681(48)
C_0	8299.0882(45)	8299.4517(13)	−0.3635(47)
$\Delta_N \times 10^3$	37.3937(159)	36.573(37)	0.821(40)
Δ_{NK}	0.181509(111)	0.18544(51)	−0.00393(52)
Δ_K	2.394778(270)		
$\delta_N \times 10^3$	4.5481(87)	4.566(49)	−0.018(50)
δ_K	0.18323(228)		
ϵ_{aa}	−1224.7306(40)	−1224.611(80)	−0.120(80)
ϵ_{bb}	−101.53380(183)	−101.5335(32)	−0.0003(37)
ϵ_{cc}	−3.78785(174)	−3.7870(30)	0.0008(35)
$\lvert\epsilon_{ab} + \epsilon_{ba}\rvert/2$	41.154(74)	41.25(13)	−0.10(15)
a_F	0.46216(161)	0.4607(28)	0.0015(32)
T_{aa}	1.2970(32)	1.2972(55)	−0.0002(64)
T_{bb}	−1.08913(277)	−1.0893(47)	0.0002(55)
$\Delta_N^S \times 10^3$	0.788(64)	0.71(11)	0.08(13)
Δ_{NK}^S	0.04933(74)	0.0451(19)	0.0042(20)
Δ_K^S	0.108 04(216)		
χ_{aa}	0.0126(44)	−0.0042(78)	0.0168(90)
χ_{bb}	0.1556(48)	0.1376(74)	0.0180(88)
Δ[b]	−0.0372	−0.0422	0.0050
fitted transitions	153	74	
rms (MHz)	0.051	0.0076	

[a] 1σ uncertainties in the unit of the last significant digit are included in parentheses. [b] Inertial defect (amu·Å^2).

extrapolation from the previous microwave work. The fast-sweep technique eased the search problem, as it could cover a wide (≥1 GHz) spectral range in less than an hour. The large shifts between the measured spectra and the extrapolation from microwave studies are primarily caused by the lack of inclusion of some quartic centrifugal distortion constants in the analysis of the microwave spectra. In the previous microwave studies, only $K_a = 1 \leftarrow 0$ transitions were detected, leading to the undetermined centrifugal distortion constants Δ_K and δ_K. Once higher K_a levels were accessed, these centrifugal distortion constants could be added in the analysis presented here. From the comparisons shown in Tables 1 and 2, it can be seen that the centrifugal distortion constants associated with the angular momentum operator on the primary axis $\hat{N}_a$, namely, Δ_{NK}, Δ_K, δ_K, Δ_{NK}^S, and Δ_K^S, are now well-defined. The inclusion of these additional centrifugal distortion constants also led to significant changes in the rotational constants A, B, and C, especially the A constant, from the values reported in previous studies. As expected, the change of the rotational constants also leads to a change in the inertial defect, but only by a small amount. Most of the spin−orbit interaction, magnetic dipole hyperfine interaction, and electric quadrupole hyperfine interaction terms have not changed within their respective statistical uncertainties.

The centrifugal distortion constants Δ_K and δ_K are significantly larger compared to the other centrifugal distortion constants Δ_N, Δ_{NK}, and δ_N. This result indicates the large dependency of HO_3 geometry on the rotational angular momentum along the principle axis. A similar trend was observed in the *trans*-HOCO radical,[45] though the C−O bond in HOCO was found to be much shorter than the O−O bond in HO_3. These large values for Δ_K and δ_K may provide additional benchmarks for theoretical calculations of the geometry and multidimensional potential energy surface for HO_3, since the distortion tensor relies on the estimation of the moment of inertia gradient and the force field.

The behavior of DO_3 is similar to that of HO_3. Because of the heavier deuterium nucleus, the shift of DO_3 constants in this work from the previous study is systematically smaller than the shift of HO_3 constants.

In addition to the interesting results found for HO_3 and DO_3, additional spectral lines were observed for other species produced in the discharge. In the previous study,[13] OH, H_2O−OH, H_2O−O_2, $(H_2O)_2$, and O_3 were also detected using similar discharge conditions to those used in this experiment. Our experiment is consistent with the previous results, as we saw strong transitions from HO_2, H_2O_2, O_3, H_2O, O_2 (both $^3\Sigma$ and $^1\Delta$), and Ar−H_2O dimer. The spectral features of these known species were excluded from the analysis of the HO_3 spectrum and are not plotted in Figure 6 (except for Ar−H_2O). In particular, Ar−H_2O was confirmed by a comparison with the spectrum of a water and Ar mixture. The Ar−H_2O vibrational−rotational-tunneling spectrum has been studied previously.[46−50] Unfortunately, no experimental data were available in the frequency range of this experiment. We therefore measured the Ar−H_2O spectrum separately to clean up the list of unidentified lines in our HO_3 spectra. The details of the Ar−H_2O spectrum are beyond the scope of this paper and will be the subject of a future manuscript.

Despite the prevalence of Ar−H_2O lines in the spectrum, this dimer can only partially reproduce the unidentified lines shown in Figure 6. Consequently, it is likely that at least one additional species was created in the discharge. These spectral lines persisted when Ar was replaced by He or even completely removed in the expansion; as such, the carrier is neither an Ar cluster nor a He cluster. The splitting pattern of these unidentified lines indicates a radical species. Future work will focus on determining the identity of this new species. Meanwhile, this new finding illustrates the capacity of the

DOI: 10.1021/acs.jpca.5b09624
J. Phys. Chem. A 2016, 120, 657−667

Table 3. Estimation of Column Density Upper Limit of HO_3 in Astronomical Sources[a]

source	right ascension	declination	column density (cm^{-2})	temperature (K)	FWHM ($km \cdot s^{-1}$)
W3(H_2O)	02:27:04.61	+61:52:25.0	$\leq 6.9 \times 10^{13}$	48.9	6.6
L1448MM-1	03:25:38.81	+30:33:00.5	$\leq 2.4 \times 10^{12}$	17.7	1.3
NGC 1333 IRAS 2A	03:28:55.40	+31:14:35.0	$\leq 3.2 \times 10^{12}$	22.4	3.4
NGC 1333 IRAS 2B	03:28:57.24	+31:11:13.9	$\leq 9.0 \times 10^{11}$	10[b]	1[c]
NGC 1333 IRAS 4A	03:29:10.49	+31:13:31.0	$\leq 2.2 \times 10^{12}$	18.9	9.6
NGC 1333 IRAS 4B	03:29:11.99	+31:13:08.9	$\leq 3.2 \times 10^{13}$	20.0	5.5
B1-b	03:33:20.80	+31:07:40.0	$\leq 1.8 \times 10^{14}$	9.9	1.2
Orion-KL	05:35:14.16	−05:22:21.5	$\leq 1.2 \times 10^{15}$	80.6	9.4
NGC 2264	06:41:00.00	+09:52:48.0	$\leq 3.1 \times 10^{13}$	20.4	4.5
NGC6334−29	17:19:57.00	−35:57:51.0	$\leq 4.1 \times 10^{13}$	49.6	5.4
NGC6334−38	17:20:18.00	−35:54:42.0	$\leq 5.2 \times 10^{12}$	26.4	3.5
NGC6334−43	17:20:23.00	−35:55:55.0	$\leq 1.3 \times 10^{13}$	16.0	3.1
NGC6334-IN	17:20:55.00	−35:45:40.0	$\leq 8.8 \times 10^{13}$	20.2	3.9
GCM + 0.693−0.027	17:47:21.86	−28:21:27.0	$\leq 3.0 \times 10^{15}$	10[b]	14.1[d]
GAL 010.47 + 00.03	18:08:38.40	−19:51:51.8	$\leq 2.1 \times 10^{14}$	62.0	10.8
GAL 12.21−0.10	18:12:39.70	−18:24:20.9	$\leq 2.0 \times 10^{13}$	28.9	8.2
GAL 012.91−00.26	18:14:39.00	−17:52:03.0	$\leq 4.9 \times 10^{12}$	29.4	4.9
HH 80/81	18:19:12.30	−20:47:27.5	$\leq 1.5 \times 10^{12}$	19.0	2.4
GAL 19.61−0.23	18:27:37.99	−11:56:42.0	$\leq 5.2 \times 10^{13}$	53.7	9.0
GAL 24.33 + 0.11	18:35:08.14	−7:35:8.14	$\leq 1.9 \times 10^{12}$	18.2	4.7
GAL 24.78 + 0.08	18:36:12.00	−7:13:12.0	$\leq 2.1 \times 10^{13}$	38.0	7.2
GAL 29.96−0.02	18:46:3.92	−2:39:21.9	$\leq 5.5 \times 10^{14}$	10[b]	1.6[e]
GAL 31.41 + 0.31	18:47:34.61	−01:12:42.8	$\leq 2.7 \times 10^{13}$	79.1	7.4
GAL 34.3 + 00.2	18:53:18.54	+01:14:57.9	$\leq 3.7 \times 10^{13}$	45.8	6.8
GAL 45.47 + 0.05	19:14:25.60	+11:09:26.0	$\leq 5.2 \times 10^{11}$	15.1	4.6
W51	19:23:43.77	+14:30:25.9	$\leq 6.7 \times 10^{13}$	49.0	9.2
GAL 75.78 + 0.34	20:21:44.09	+37:26:39.8	$\leq 4.2 \times 10^{12}$	28.0	4.2
W75N	20:38:35.90	+42:37:22.1	$\leq 1.2 \times 10^{14}$	42.7	5.6
DR21(OH)	20:39:01.10	+42:22:49.1	$\leq 3.4 \times 10^{13}$	39.0	6.0
L1157 MM	20:39:06.41	+68:02:12.8	$\leq 1.7 \times 10^{13}$	14.3	5.8
NGC 7538	23:13:45.70	+61:28:21.0	$\leq 3.1 \times 10^{11}$	19.0	3.7

[b]No temperature information is available. The temperature was assumed to be 10 K. [c]fwhm assumed to be 3 times the channel width, which is ∼1 km· s^{-1}. [d]fwhm of CS. [e]fwhm of CO. [a]The listed temperature and fwhm are the weighted average values from other molecules fitted in each source and were fixed during the analysis for HO_3.

fast-sweep technique. Since this technique allows scanning for tens of GHz in a day under normal experimental conditions, it makes blind searches feasible even without any spectroscopic prediction. This opens the possibility of discovering new spectral features in the millimeter−submillimeter range, which could not be done easily before with the conventional point-by-point spectral acquisition technique.

■ COMPARISON TO OBSERVATIONS

To begin the astronomical search for HO_3, we compared the laboratory spectra discussed above with a set of spectral observations toward 32 star-forming regions taken using the Caltech Submillimeter Observatory (CSO) between 2007 September and 2013 June. (The CSO is operated by the California Institute of Technology, previously under contract from the National Science Foundation.) Both a prototype wideband receiver[51,52] and the facility wideband receiver[53] were used for these observations. For the observations using the prototype receiver, the facility acousto-optical spectrometer was used, and the resultant spectra had 4 GHz bandwidth and ∼0.65 MHz channel width. For the observations using the facility receiver, the facility fast Fourier transform spectrometer (FFTS) was used, and the resultant spectra had 4 GHz bandwidth and ∼0.27 MHz channel width. A set of rest frequencies with 4 GHz separation was used in the range of 223.192−251.192 GHz. A set of IF offsets of 4.254, 6.754, 5.268, and 7.795 GHz were applied to each rest frequency to ensure a minimum sampling redundancy of six for each frequency point in the spectra; additional IF offsets of 6.283, 4.752, 5.767, and 7.269 were applied to the lowest two frequency settings. This redundancy ensured sufficient sampling for full deconvolution of the double-sideband (DSB) spectra. A chopper wheel was used for intensity calibration to place the spectra on the antenna temperature scale, T_a^*. The chopper wheel was operated at 1.1 Hz with a throw of either 70 ± 8 or 90 ± 8 arcsec. A noise level of 30 mK was obtained for each source through adjustment of integration times based on the system temperature during observations. Pointing accuracy was within 5 arcsec each night; the pointing was checked at a minimum of every 2 h, and spectral intensities were compared to those of previous nights to ensure consistency. The full-width-half-power beam sizes at 230 GHz were 33.4 and 35.54 arcsec for the prototype and facility receivers, respectively. Data reduction and deconvolution were performed using the CLASS software package in the GILDAS suite (Institut de Radioastronomie Millimetrique, Grenoble, France). DSB spectra were baseline-corrected, noise features were removed, strong spectral features were masked, and spectra were resampled with 1 MHz channel spacing before deconvolution. Spectra were rescaled to the main beam

DOI: 10.1021/acs.jpca.5b09624
J. Phys. Chem. A 2016, 120, 657−667

temperature scale, T_{mb}, using a beam efficiency determined through observations of the planets to be 0.60 ± 0.09 for both receivers. The final spectra have noise levels of ∼25 mK.

The Global Optimization and Broadband Analysis Software for Interstellar Chemistry (GOBASIC) program was then used to analyze the astronomical observations through comparison with the spectral line catalog generated from the molecular parameters given in Table1. The details of the program are described elsewhere.[54] For each observational spectrum, the brightness temperature was calibrated by the antenna efficiency but was not further calibrated for beam dilution because the spatial distribution for HO_3 is unknown for all sources. Before analyzing the spectra for HO_3, spectroscopic features of other commonly found interstellar molecules were fitted. Some common molecules included in this preliminary analysis are CS isotopologues, methanol, SO_2, CH_3CN, dimethyl ether, and methyl formate. The exact molecules included varied based on the unique molecular composition of each astronomical source. After this preliminary analysis was completed, a trial fit for HO_3 was conducted using the updated HO_3 line catalog. The temperature and full-width-half-maximum (FWHM) of the trial fit was constrained to the weighted average of these values found for other molecules in that source, with the weighting set as the reciprocal of their estimated uncertainty. Unfortunately, no transitions of *trans*-HO_3 were found in any of these observational line surveys. Therefore, the fitted column density was interpreted as an upper limit for HO_3 column density in each source. The results of this analysis are summarized in Table 3. No information is included here for Sgr B2(N), because severe line confusion and blending precluded analysis for HO_3.

The results of this initial search for HO_3 are not surprising based on the difficulties faced in detecting O_2 in interstellar sources. Also, HO_3 detection might be even more challenging in this particular set of sources since the observations focused on warmer regions of star formation, where weakly bound clusters might not be prevalent. Nonetheless, there are several cold prestellar cores included in this sample, and yet HO_3 was not detected in any of them. Despite this lack of detection, there is still a possibility for HO_3 detection in future observations. Recent advances in radio interferometry led to much higher sensitivity levels than those achieved in these observations. For example, only a 10 min integration using the Atacama Large Millimeter/Submillimeter Array (ALMA) at 240 GHz with 1 MHz bandwidth would achieve a noise level of 10 mK (calculated using the ALMA sensitivity calculator at https://almascience.eso.org/about-alma/proposing/sensitivity-calculator). Therefore, detection of HO_3 may be possible with more sensitive observations of colder regions. In particular, HO_3 may be detectable in other regions with higher O_2 abundance such as O-rich stellar envelopes.

CONCLUSIONS

We have presented the measurement of pure rotational transitions of HO_3 and DO_3 in the 70−450 GHz frequency range. A large discrepancy was found between these new experimental measurements and the spectral extrapolation from previous FTMW studies.[12,13] This discrepancy was fully explained by the inclusion of additional quartic centrifugal distortion constants in the Hamiltonian. Molecular constants were fitted using the new experimental results and were used to generate a more reliable submillimeter spectral extrapolation for these two radicals.

Along with the reported HO_3 and DO_3 spectra, we have benchmarked a fast-sweep spectroscopic technique that facilitated the search for HO_3 transitions. This technique is well-suited for spectral searches for unknown molecular transitions in a broad frequency range in the millimeter−submillimeter regime. Using this technique, we also revealed new spectral features arising from the discharge chemistry for HO_3 production. Some of these new spectral features have been identified as arising from Ar−H_2O dimer, but the carrier of other spectral features remains unidentified.

To address the possible importance of weakly bound clusters like HO_3 in the astrochemistry of star-forming regions, we attempted a preliminary search for HO_3 in 32 astronomical sources. Unfortunately, no HO_3 was detected in these line surveys, likely due to the presumably low abundance of HO_3. Nonetheless, upper limits were estimated for each of these sources. Additionally, the updated spectral line catalog based on new experimental measurements presented here is expected to guide new astronomical searches in other sources that have high expected abundances of HO_3.

ASSOCIATED CONTENT

Supporting Information

The Supporting Information is available free of charge on the ACS Publications website at DOI: 10.1021/acs.jpca.5b09624.

The fit files associated with the HO_3 and DO_3 fits using the CALPGM program. (ZIP)

AUTHOR INFORMATION

Corresponding Author

*E-mail: swidicu@emory.edu.

Notes

The authors declare no competing financial interest.

Biographies

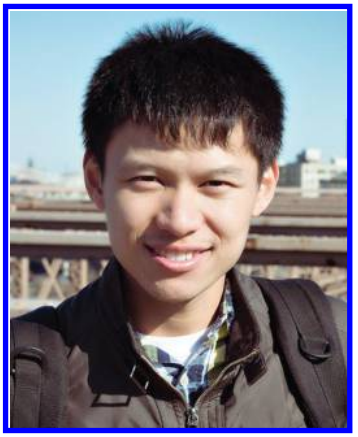

Luyao Zou received his B.S. in Chemistry from Fudan University, Shanghai, China, in 2012. He is currently a Ph.D. student in Prof. Widicus Weaver's research group at Emory University. His main research interests are millimeter−submillimeter spectroscopy on radicals and ions of astrochemical importance and analysis of astronomical observations.

DOI: 10.1021/acs.jpca.5b09624
J. Phys. Chem. A 2016, 120, 657−667

Brian Hays received his B.S. in Chemistry from Loyola University New Orleans in 2010 and his Ph. D. from Emory University in 2015. He is currently a postdoctoral scholar in the laboratory of Prof. Timothy Zwier at Purdue University. His research focuses on rotational spectroscopy of reactive species and spectrometer development.

Susanna Widicus Weaver is an Associate Professor of Chemistry at Emory University. She received a B.S. in Chemistry from Illinois Wesleyan University in 2000, and a Ph.D. in Chemistry from the California Institute of Technology in 2005. She was a Chemistry and Astronomy postdoctoral scholar at the University of Illinois. She began her career at Emory University in 2008 and was granted tenure in 2014. Her research integrates laboratory spectroscopy, observational astronomy, and astrochemical modeling to study prebiotic chemistry during star and planet formation.

■ ACKNOWLEDGMENTS

The laboratory investigations were supported by the National Science Foundation CAREER Award No. CHE-1150492. The authors thank M. Correa for his help in collecting some of the HO_3 data and M. McCarthy for helpful discussions pertaining to the HO_3 experiments and analysis. The observational astronomy was supported by S.L.W.W.'s startup funds, provided by Emory Univ., and by the Emory Summer Undergraduate Research Program. The authors thank N. Wehres, T. Cross, M. Rad, J. Laas, and J. Kroll for their work with the CSO observations; M. Sumner, F. Rice, and J. Zmuidzinas for design and implementation of the prototype receiver; D. Lis, M. Emprechtinger, B. McGuire, P. Schilke, and C. Comito for their guidance and input on the analysis of double-sideband observations; and T. Phillips, R. Chamberlin, S. Radford, E. Bufil, and the rest of the CSO staff for their guidance and support. The authors also thank the support staff from Emory. This material is partially based upon work at the Caltech Submillimeter Observatory, which was operated by the California Institute of Technology under cooperative agreement with the National Science Foundation (AST-0838261).

■ REFERENCES

(1) Goldsmith, P. F.; Liseau, R.; Bell, T. A.; Black, J. H.; Chen, J.-H.; Hollenbach, D.; Kaufman, M. J.; Li, D.; Lis, D. C.; Melnick, G.; et al. Herschel Measurements of Molecular Oxygen in Orion. *Astrophys. J.* **2011**, *737*, 96.

(2) Liseau, R.; Goldsmith, P. F.; Larsson, B.; Pagani, L.; Bergman, P.; Le Bourlot, J.; Bell, T. A.; Benz, A. O.; Bergin, E. A.; Bjerkeli, P.; et al. Multi-line Detection of O_2 toward ρ Ophiuchi A. *Astron. Astrophys.* **2012**, *541*, A73.

(3) Melnick, G. J.; Tolls, V.; Goldsmith, P. F.; Kaufman, M. J.; Hollenbach, D. J.; Black, J. H.; Encrenaz, P.; Falgarone, E.; Gerin, M.; Hjalmarson, Å.; et al. Herschel Search for O_2 toward the Orion Bar. *Astrophys. J.* **2012**, *752*, 26.

(4) Chen, J.-H.; Goldsmith, P. F.; Viti, S.; Snell, R.; Lis, D. C.; Benz, A.; Bergin, E.; Black, J.; Caselli, P.; Encrenaz, P.; et al. Herschel HIFI Observations of O_2 toward Orion: Special Conditions for Shock Enhanced Emission. *Astrophys. J.* **2014**, *793*, 111.

(5) Whittet, D. C. B. Oxygen Depletion in the Interstellar Medium: Implications for Grain Models and the Distribution of Elemental Oxygen. *Astrophys. J.* **2010**, *710*, 1009.

(6) Klemperer, W.; Vaida, V. Molecular Complexes in Close and Far Away. *Proc. Natl. Acad. Sci. U. S. A.* **2006**, *103*, 10584−10588.

(7) Cooper, P. D.; Moore, M. H.; Hudson, R. L. Infrared Detection of HO_2 and HO_3 Radicals in Water Ice. *J. Phys. Chem. A* **2006**, *110*, 7985−7988.

(8) Zheng, W.; Jewitt, D.; Kaiser, R. I. Mechanistical Studies on the Formation of Isotopomers of Hydrogen Peroxide (HOOH), Hydrotrioxy (HOOO), and Dihydrogentrioxide (HOOOH) in Electron-irradiated $H_2{}^{18}O/O_2$ Ice Mixtures. *Phys. Chem. Chem. Phys.* **2007**, *9*, 2556−2563.

(9) Le Picard, S. D.; Tizniti, M.; Canosa, A.; Sims, I. R.; Smith, I. W. M. The Thermodynamics of the Elusive HO_3 Radical. *Science* **2010**, *328*, 1258−1262.

(10) Suma, K.; Sumiyoshi, Y.; Endo, Y. Force-field Calculation and Geometry of the HOOO Radical. *J. Chem. Phys.* **2013**, *139*, 094301−8.

(11) Varandas, A. J. C. Ab Initio Treatment of Bond-Breaking Reactions: Accurate Course of HO_3 Dissociation and Revisit to Isomerization. *J. Chem. Theory Comput.* **2012**, *8*, 428−441.

(12) Suma, K.; Sumiyoshi, Y.; Endo, Y. The Rotational Spectrum and Structure of the HOOO Radical. *Science* **2005**, *308*, 1885−1886.

(13) McCarthy, M. C.; Lattanzi, V.; Kokkin, D.; Martinez, O.; Stanton, J. F. On the Molecular Structure of HOOO. *J. Chem. Phys.* **2012**, *136*, 034303−10.

(14) Murray, C.; Derro, E. L.; Sechler, T. D.; Lester, M. I. Weakly Bound Molecules in the Atmosphere: A Case Study of HOOO. *Acc. Chem. Res.* **2009**, *42*, 419−427. PMID: 19113857.

(15) Speranza, M. Structure, Stability, and Reactivity of Cationic Hydrogen Trioxides and Thermochemistry of their Neutral Analogs. A Fourier-Transform Ion Cyclotron Resonance Study. *Inorg. Chem.* **1996**, *35*, 6140−6151.

(16) Speranza, M. Stable vs Metastable HOOO. An Experimental Solution for an Evergreen Theoretical Dilemma. *J. Phys. Chem. A* **1998**, *102*, 7535−7536.

(17) Derro, E. L.; Sechler, T. D.; Murray, C.; Lester, M. I. Observation of 1+n Combination Bands of the HOOO and DOOO Radicals Using Infrared Action Spectroscopy. *J. Chem. Phys.* **2008**, *128*, 244313.

(18) Cacace, F.; de Petris, G.; Pepi, F.; Troiani, A. Experimental Detection of Hydrogen Trioxide. *Science* **1999**, *285*, 81−82.

(19) Nelander, B.; Engdahl, A.; Svensson, T. The HOOO Radical. A Matrix Isolation Study. *Chem. Phys. Lett.* **2000**, *332*, 403−408.

DOI: 10.1021/acs.jpca.5b09624
J. Phys. Chem. A 2016, 120, 657−667

(20) Derro, E. L.; Murray, C.; Sechler, T. D.; Lester, M. I. Infrared Action Spectroscopy and Dissociation Dynamics of the HOOO Radical. *J. Phys. Chem. A* **2007**, *111*, 11592−11601. PMID: 17503792.
(21) Murray, C.; Derro, E. L.; Sechler, T. D.; Lester, M. I. Stability of the Hydrogen Trioxy Radical via Infrared Action Spectroscopy. *J. Phys. Chem. A* **2007**, *111*, 4727−4730. PMID: 17503792.
(22) Derro, E. L.; Sechler, T. D.; Murray, C.; Lester, M. I. Infrared Action Spectroscopy of the OD Stretch Fundamental and Overtone Transitions of the DOOO Radical. *J. Phys. Chem. A* **2008**, *112*, 9269−9276. PMID: 18507450.
(23) Liang, T.; Magers, D. B.; Raston, P. L.; Allen, W. D.; Douberly, G. E. Dipole Moment of the HOOO Radical: Resolution of a Structural Enigma. *J. Phys. Chem. Lett.* **2013**, *4*, 3584−3589.
(24) Raston, P. L.; Liang, T.; Douberly, G. E. Infrared Spectroscopy of HOOO and DOOO in ^{4}He Nanodroplets. *J. Chem. Phys.* **2012**, *137*, 184302.
(25) Varandas, A. J. C.; Yu, H. G. Double Many-body Expansion Potential Energy Surface for Ground-state HO_3. *Mol. Phys.* **1997**, *91*, 301−318.
(26) Denis, P. A.; Kieninger, M.; Ventura, O. N.; Cachau, R. E.; Diercksen, G. H. Complete Basis Set and Density Functional Determination of the Enthalpy of Formation of the Controversial HO_3 Radical: a Discrepancy Between Theory and Experiment. *Chem. Phys. Lett.* **2002**, *365*, 440−449.
(27) Mansergas, A.; Anglada, J. M.; Olivella, S.; Ruiz-Lopez, M. F.; Martins-Costa, M. On the Nature of the Unusually Long OO Bond in HO_3 and HO_4 Radicals. *Phys. Chem. Chem. Phys.* **2007**, *9*, 5865−5873.
(28) Braams, B. J.; Yu, H.-G. Potential Energy Surface and Quantum Dynamics Study of Rovibrational States for HO_3 (X^2A''). *Phys. Chem. Chem. Phys.* **2008**, *10*, 3150−3155.
(29) Varner, M. E.; Harding, M. E.; Gauss, J.; Stanton, J. F. On the Geometry of the HO_3 Radical. *Chem. Phys.* **2008**, *346*, 53−55.
(30) Denis, P. A.; Ornellas, F. R. Theoretical Characterization of Hydrogen Polyoxides: HOOH, HOOOH, HOOOOH, and HOOO. *J. Phys. Chem. A* **2009**, *113*, 499−506.
(31) Varner, M. E.; Harding, M. E.; Vázquez, J.; Gauss, J.; Stanton, J. F. Dissociation Energy of the HOOO Radical. *J. Phys. Chem. A* **2009**, *113*, 11238−11241. PMID: 19785472.
(32) Anglada, J. M.; Olivella, S.; Solé, A. On the Dissociation of Ground State trans-HOOO Radical: A Theoretical Study. *J. Chem. Theory Comput.* **2010**, *6*, 2743−2750.
(33) Beames, J. M.; Lester, M. I.; Murray, C.; Varner, M. E.; Stanton, J. F. Analysis of the HOOO Torsional Potential. *J. Chem. Phys.* **2011**, *134*, 044304.
(34) Varandas, A. J. C. IS HO_3 Minimum cis or trans? An Analytic Full-dimensional ab initio Isomerization Path. *Phys. Chem. Chem. Phys.* **2011**, *13*, 9796−9811.
(35) Varandas, A. J. C. On the Stability of the Elusive HO_3 Radical. *Phys. Chem. Chem. Phys.* **2011**, *13*, 15619−15623.
(36) Hoy, E. P.; Schwerdtfeger, C. A.; Mazziotti, D. A. Relative Energies and Geometries of the cis- and trans-HO_3 Radicals from the Parametric 2-Electron Density Matrix Method. *J. Phys. Chem. A* **2013**, *117*, 1817−1825.
(37) McCarthy, M. C.; Chen, W.; Travers, M. J.; Thaddeus, P. Microwave Spectra of 11 Polyyne Carbon Chains. *Astrophys. J., Suppl. Ser.* **2000**, *129*, 611−623.
(38) Grabow, J.-U.; Palmer, E. S.; McCarthy, M. C.; Thaddeus, P. Supersonic-jet Cryogenic-resonator Coaxially Oriented Beam-resonator Arrangement Fourier Transform Microwave Spectrometer. *Rev. Sci. Instrum.* **2005**, *76*, 093106.
(39) Kaur, D.; de Souza, A. M.; Wanna, J.; Hammad, S. A.; Mercorelli, L.; Perry, D. S. Multipass Cell for Molecular Beam Absorption Spectroscopy. *Appl. Opt.* **1990**, *29*, 119−124.
(40) Laas, J. C.; Hays, B. M.; Widicus Weaver, S. L. Multipass Millimeter/Submillimeter Spectrometer to Probe Dissociative Reaction Dynamics. *J. Phys. Chem. A* **2013**, *117*, 9548−9554.
(41) Petkie, D. T.; Goyette, T. M.; Bettens, R. P. A.; Belov, S. P.; Albert, S.; Helminger, P.; De Lucia, F. C. A Fast Scan Submillimeter Spectroscopic Technique. *Rev. Sci. Instrum.* **1997**, *68*, 1675−1683.
(42) Park, G. B.; Steeves, A. H.; Kuyanov-Prozument, K.; Neill, J. L.; Field, R. W. Design and Evaluation of a Pulsed-jet Chirped-pulse Millimeter-wave Spectrometer for the 70−102 GHz Region. *J. Chem. Phys.* **2011**, *135*, 024202.
(43) Melnik, D. G.; Gopalakrishnan, S.; Miller, T. A.; De Lucia, F. C.; Belov, S. Submillimeter Wave Vibration-rotation Spectroscopy of Ar−CO and Ar−ND_3. *J. Chem. Phys.* **2001**, *114*, 6100−6106.
(44) Pickett, H. M. The Fitting and Prediction of Vibration-rotation Spectra with Spin Interactions. *J. Mol. Spectrosc.* **1991**, *148*, 371−377.
(45) Sears, T. J.; Radford, H. E.; Moore, M. A. b−dipole Transitions in trans−HOCO Observed by Far Infrared Laser Magnetic Resonance. *J. Chem. Phys.* **1993**, *98*, 6624−6631.
(46) Cohen, R. C.; Busarow, K. L.; Laughlin, K. B.; Blake, G. A.; Havenith, M.; Lee, Y. T.; Saykally, R. J. Tunable Far Infrared Laser Spectroscopy of Van der Waals Bonds: Vibration−rotation−tunneling Spectra of Ar-H_2O. *J. Chem. Phys.* **1988**, *89*, 4494−4504.
(47) Cohen, R. C.; Busarow, K. L.; Lee, Y. T.; Saykally, R. J. Tunable Far Infrared Laser Spectroscopy of Van der Waals Bonds: The Intermolecular Stretching Vibration and Effective Radial Potentials for Ar−H_2O. *J. Chem. Phys.* **1990**, *92*, 169−177.
(48) Cohen, R. C.; Saykally, R. J. Multidimensional Intermolecular Dynamics from Tunable Far−infrared Laser Spectroscopy: Angular-radial Coupling in the Intermolecular Potential of Argon−H_2O. *J. Chem. Phys.* **1991**, *95*, 7891−7906.
(49) Fraser, G.; Lovas, F.; Suenram, R.; Matsumura, K. Microwave Spectrum of Ar-H_2O: Dipole Moment, Isotopic Studies, and ^{17}O Quadrupole Coupling Constants. *J. Mol. Spectrosc.* **1990**, *144*, 97−112.
(50) Germann, T. C.; Gutowsky, H. S. Nuclear Hyperfine Interactions and Dynamic State of H_2O in Ar-H_2O. *J. Chem. Phys.* **1993**, *98*, 5235−5238.
(51) Rice, F.; Sumner, M.; Zmuidzinas, J.; Hu, R.; LeDuc, H. G.; Harris, A. I.; Miller, D. SIS Mixer Design for a Broadband Millimeter Spectrometer Suitable for Rapid Line Surveys and Redshift Determinations. *Proc. SPIE* **2002**, *4855*, 301−311.
(52) Kaul, A. B.; Bumble, B.; Lee, K. A.; LeDuc, H. G.; Rice, F.; Zmuidzinas, J. Fabrication of Wide−IF 200−300 GHz Superconductor-insulator−superconductor Mixers with Suspended Metal Beam Leads Formed on Silicon−on−insulator. *J. Vac. Sci. Technol., B: Microelectron. Process. Phenom.* **2004**, *22*, 2417−2422.
(53) Kooi, J. W.; Kovacs, A.; Sumner, M. C.; Chattopadhyay, G.; Ceria, R.; Miller, D.; Bumble, B.; Leduc, H. G.; Stern, J. A.; Phillips, T. G. A 275−425−GHz Tunerless Waveguide Receiver Based on AlN−Barrier SIS Technology. *IEEE Trans. Microwave Theory Tech.* **2007**, *55*, 2086−2096.
(54) Radhuber, M. L.; Zou, L.; Sanders, J. L., III; Weaver, S. L. W. Global Optimization and Broadband Analysis Software for Interstellar Chemistry (GOBASIC). *Astron. Astrophys.* **2016**, *585*, A23.

NOTE ADDED AFTER ISSUE PUBLICATION

This paper was published with production errors in Table 3 in the version published on the Web on December 28, 2015. The corrected version was published on March 14, 2016.

DOI: 10.1021/acs.jpca.5b09624
J. Phys. Chem. A 2016, 120, 657−667